E-ISSN: 2997-9382
American Journal of Technology Advancement
https://semantjournals.org/index.php/AJTA

| Research Article

Check for updates

The Effect of the Different Coefficient of Friction in Clamp Dies on the Pipe Deformation

Hassan Raheem Hassan
College of Engineering, Al-Shatrah University, Thi-Qar, Iraq

Annotation

Bent tube is one type of tube forming process whereby the movement position of the neutral axis shifts to the inner arc and the change of wall thickness distribution occurs. The present paper investigates how these phenomena evolve across the phenomenon and determine the effects of a different coefficient of friction between 0.1 and 0.5 and bending angles ranging from 15° to 90°. Finite element analysis using ABAQUS software has been used to study the behavior of both stainless steel and steel alloys. The findings show that stainless steel has required steady performance with little changes trend in the wall thickness and neutral axis displacement. In comparison, steel alloys are found to be more sensitive to friction, inducing significantly larger changes in the wall thickness and more obvious displacement of the neutral axis, especially at larger bending angles and friction coefficients of strip curvature. The paper is concerned with an examination of material responses through a comparative analysis, focusing on the role of friction to command the structural end results of the tube bending process.

Keywords: Try to vary the wording of each phrase if possible for the sake of differentiation, but keep the meaning.

Introduction

The bending of thin-walled tubes has been widely applied in the fields of automotive, aviation, space, and so forth. Because of its potential in meeting demands for lightweight and high strength, it has become a hot research issue in novel metal forming technology [1–3, 33–34]. In the past, in the case of forming a pipe member, an entire shape such as elastic return after bending [4-6], a distortion in a cross sectional shape [7-9] and a thinning [10-12], [35, 36] and the like of various deformation flaws are imposed. Exact prediction of wall thinning is essential for the tubing industry, as it directly impacts the pressure-resistance capabilities of bent tubes. Therefore, precise control over the bending process is required to maintain wall thinning within specified limits; otherwise, the pipeline may be susceptible to failure during operation [13–15]. In the NC bending process, a tube is positioned within the bending machine and clamped between an inner and outer clamp die. Both dies rotate around the bending axis, shaping the tube to match the radius of the bending die. During the forming process, the pressure die (or slide piece) absorbs the radial stresses generated, particularly benefiting applications involving mandrel bending. This

configuration enhances the quality of thin-walled tubes, achieving precise bends with minimal deformation even at small radii [16]. Figure 1a, for instance, illustrates a standard rotary draw bending setup, emphasizing the crucial role of each component. After bending, the geometry of the tube undergoes notable changes, including the shifting of the neutral axis toward the inner arc. Initially aligned with the tube natural center, the neutral axis moves inward during bending, creating a new bending radius, R' , distinct from the original bending radius, R_b . This shift also affects the tube wall thickness distribution, resulting in thinning at the outer arc and thickening at the inner arc. The extent of this distribution depends on various factors, including the material type and the friction coefficients between the die components involved.

The breaking down of the loads in rotational compressive bending is complicated since, an axial load is produced without pulling of the specimen by an external load. This approach is mainly determined by bend curvature ratio i.e., ratio of tube bend radius to its external width [17]. With increasing w/D, the circumferential bending tension decreases, especially near the formability limit for narrow, thick-walled tubes. The reduction in thickness, necessary for maintaining mechanical integrity, depends closely on this ratio and on the enlargement of the outer circumference of the pipe. Higher curvature ratios and increased radial compression rates resulted in significant reduction of shape distortion and flexural stress. thereby enhancing structural stability [14,18]. Simulations and experiments on freeform bending of steel tubes indicate that adjusting feed rate and mandrel position produces distinct residual stress states, where higher feed rates induce greater interior compressive stresses and hardness, while lower feed rates increase exterior tensile stresses and decrease hardness [19].

Detecting wrinkling in thin-walled tubes during three-roll push bending is crucial, particularly for tubes with diameters close to 60 mm and wall thicknesses of 1.15 mm [20]. Monitoring vibrations and angular rates enables the identification of both localized and spread wrinkling across bending angles of up to 15 degrees. Wrinkle formation can be detected within the first 0.15 seconds of the process, allowing for immediate adjustments that enhance precision and control, ensuring high-quality results in applications requiring strict dimensional accuracy. Greater clearances between the tube and die, along with higher bending velocities, are associated with increased wrinkling severity [21]. Elevated friction coefficients also enhance the wrinkling and deformation by increasing resistance and the accumulation of stress, especially in the compressive areas of the tube [22]. Integrated lubrication and tool optimization are therefore necessary for effective handling of the fringe and hence related defects such as wrinkling and ovalization as well as for enhancing the quality of the bending operation as a whole [23,24]..

The springback greatly influences the dimensional accuracy of the bent tube, in particular the bending in complex shape. The knowledge of bending angles, FP properties and other influencing factors is important for the prediction and compensation of dimensional deviations after removal of the bending loads allowing for improved accuracy in applications with complex geometry [25,26]. An empirical equation of the springback angle based on experiment results and finite element analysis (FEA) demonstrates that the ratio of plastic modulus to elastic modulus, hardening index, bending radius, and thickness effect significantly on the springback [27]. The springback angle increases linearly with an increase of the plastic-to-elastic modulus ratio and decrease of hardening index. Furthermore, higher bending radii cause more elastic recovery, which magnifies springback, and higher bending angles and thinner wall thicknesses adds more springback [28] due to which the angular deviations rise up to 4.5 degrees and shape deviations are close to nearly 5%.

In rotary draw benders, the neutral axes of tubes move towards the inside of the arc profile, and thinning of material at the outside of the arc profile and thickening at the inside of the arc profile occur. This shift of axis has a great impact on wall thickness and strain distribution, the material properties play an important role in deciding the magnitude of movement [16]. The neutral axis of

aluminum diverges to a greater extent than stainless steel, this has an influence on the structural behavior of the tube subjected to bending loads. It is demonstrated that, as compared to compression bending, rotary draw bending can produce tighter radii with a geometrically-constant cross-section and less plastic deformation, whereas, compression bending reduces springback but there is an increased damage to the tube in ovality and wall thinning [29]. These differences emphasize that compression bending is an excellent process for products that require relatively loose tolerances, while rotary-draw bending is still the process of choice for products needing close tolerances and controlled tube shape. In this work, finite element simulations investigate the effect of coefficient of friction on material properties, neutral axis transfer and wall thickness distribution during rotary draw bending. Effects of friction coefficients (0.1-0.5) and bending angles (15-90 degree) were examined. Finite element models were developed in ABAQUS to investigate the influence of friction on deformation and damage on both stainless steel and steel alloys.

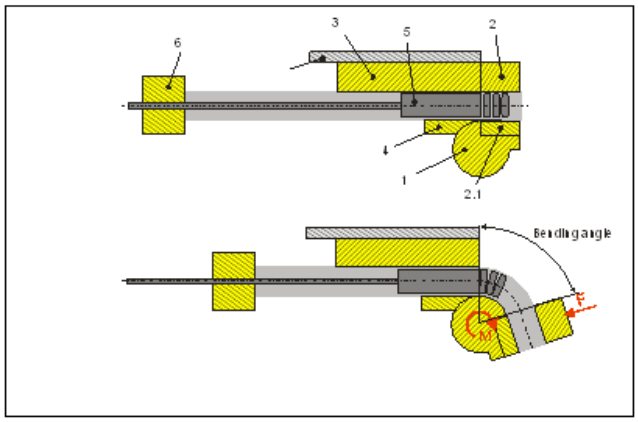

Figure 1.

Simulation techniques and boundary conditions:

Simulations were performed by building up 3D models of problem geometries in a CAD system or in pre-processor package (such as ABAQUS). The model (region of interest) were meshed carefully, as it contains core components for a very complex and time-consuming problems. The mesh and material definition was applied only to these such critical components. After the mesh generation, the model was transferred to a pre-processor, employing interfaces like The geo metrical model was first created in IGES or STEP formats. Then, the pre-processing module generated the image. All physical attributes, forces, and kinematic constraints were specified during this pre-elaboration phase. Figure 2 shows the full computational analysis approach in structural domain [12].

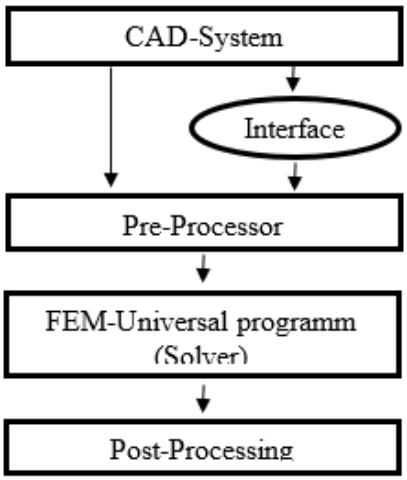

Figure 2: General Procedure of FEM [12]

A key aspect of the simulation was to grasp the material flow curves, that is needed to predict material response during bending. These curves are the result of tensile experiments carried out by the University of Siegen on flat specimens and obtained in terms of Swift criterion. Without neglecting the physical properties of the flow, it is also essential to establish the geometrical dimensions, mechanical properties and the relationships of interaction of potentially new materials before simulating them. Summary of the simulation parameters are provided in Table 1.

Tabel 1. Parameters for Simulation [16]

Parameter	Value
R_b	75mm
L_C	60mm
L_p	180mm
L_W	120mm
F_p	40KN
F_C	60KN
W (Wall thickening factor)	15
B (Bending factor)	1.8
D	35mm
t_o	1.5mm

Additional data relevant to the mandrel shaft and mandrel balls, including the necessary gap dimensions required during assembly, are provided in Table 2.

Tabel 2. Data for Manderal Balls and Manderal Shaft [16]

Manderal Diameter	Balls Number	Balls Diameter	Balls Width	Gap
35	3	35	20	1

For this study, a stainless steel alloy (1.4335) was selected for the simulation. The material properties of this alloy, alongside those of a comparative steel alloy, are detailed in Table 3.

Table3. Material Characteristics [16]

Parameter	Stainless Steel Alloy (1.4335mm)	Steel Alloy (1.008mm)
Density, (g/cm3)	7.86	7.85
Modulus of Elasticity, E (Kpa)	195	210
Strain Hardening exponent,n	0.37	0.1906
$R_{p0.2}$(MPa)	464	302.87
Rm (MPa)	707	417.32

The assignment of interaction properties, particularly the coefficients of friction between various components and the tube during the bending process, was a critical element of the simulation. The accurate determination of these coefficients is essential for replicating realistic conditions within the finite element model. Figure 3 illustrates the standard coefficients of friction applied in the model. The tools involved in the simulation included the bending die, clamp dies, pressure die, wiper die, and a universal flexing mandrel with four mandrel balls. The friction coefficient along the tube-tool interfaces was set at 0.1, except between the tube and clamp dies, where it was increased to 0.27 to account for the heightened friction in that area. The dimensions of the tools and process parameters employed in the Various important parameters, such as the bend radius

(RbR_bRb), the clamp die length (LCL_CLC), the pressure die length (LpL_pLp), and the wiper die length (LWL_WLW), were taken into account in the model. It also takes into account the wall thickness coefficient (WWW), obtained by dividing the exterior diameter of the tube by the wall thickness and bending coefficient (BBB), as the relationship between bending radius and exterior diameter of the tube. Other considerations are given by the force of the pressurizing process (FpF_pFp), the clamping force (FCF_CFC), the diameter of the tube (DDD) and its initial wall thickness (tot_oto) [30]. For more accurate simulation, the frictional coefficient between the upper and lower clamps was varied between 0.1~0.5. An external clamp die was applied 75 kN force, and a pressure die was loaded 45 kn during the simulation [16].

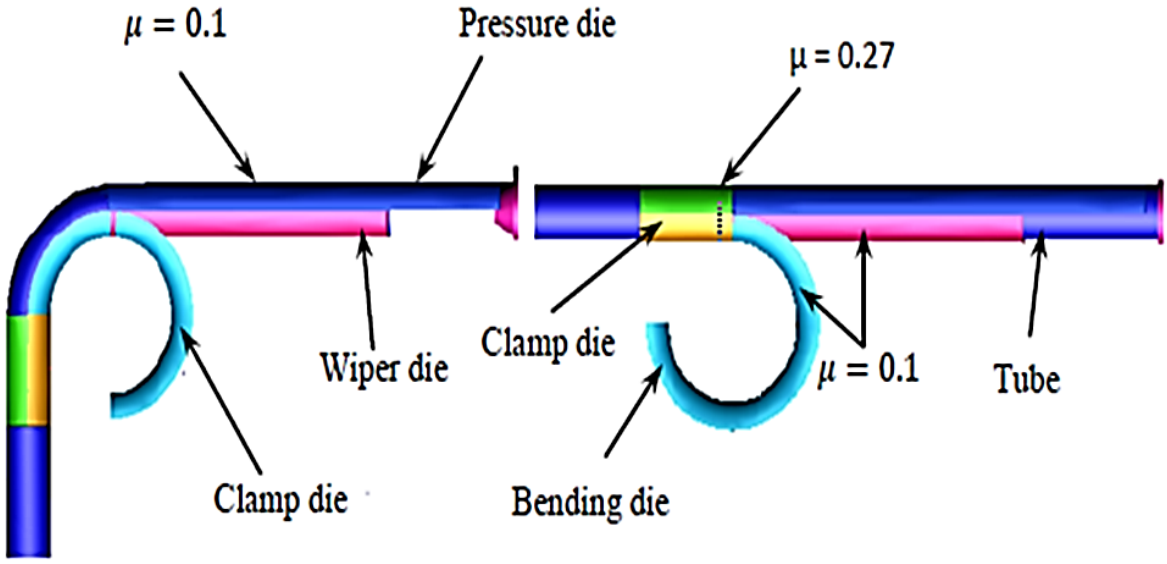

Figure 3. Finite element model with coefficient of frictions [30]

Mathematical Model:

The moment of inertia, also called the mass, angular mass, or rotational inertia, of a body is a measure of its resistance to changes in its state of motion when a torque is applied to it. Its value is the torque needed to cause a unit angular acceleration about the (chosen) rotation axis, which depends on the body's mass distribution and the axis chosen. The higher is moment of inertia, the higher is the torque required to change the body rotation velocity. This property is particularly important in rotary draw bending, an accurate industrial process used to shape tube and profiles into curves with minimum deformation or restriction of the cross section.

Rotary inertia is integral to the simulation and execution of rotary draw bending, as it directly influences the torque necessary to achieve the desired bend. The moment of inertia for a given geometry in this process can be calculated using the following expression [31]:

$$J = 1.41 + \frac{0.42}{K} \quad (1)$$

where J represents the moment of inertia and K is the geometry parameter, which encapsulates the relationship between the bending radius Rb and the average radius r of the tube cross-section. The geometry parameter K is defined by:

$$K = \frac{Rb}{2r} \quad (2)$$

With Rb =75mm, r =39mm and an analytical computed moment of inertia J =1.8468J, this result is critical in the calculation of the additional torque required to achieve a non-swell and accurate bend in the rotary draw bending process. Like with the moment of inertia, knowledge of the stress

and the strain experienced by the material during formation are also essential. The normal stress, that is the internal force per unit area, thus can be written in the form:

$$\sigma_n = \frac{F}{A} \quad (3)$$

where F is the applied force and A is the cross-sectional area. Strain, which measures the deformation of the material, is given by:

$$\varepsilon = \frac{N}{l_o} \quad (4)$$

where N is length increase and is material original length. The combined effect of these factors - moment of inertia, stress and strain - control how material responds to the application of bending moments, which can be used to design and optimize the bending process. By this way, the efficiency, accuracy and safety of the operation for rotary draw bending can be STPM to improve quality such as final product quality in relevant industrial applications.

5. Results:

In tube bending, thinning of walls is a crucial concerning factor for processing limitations, especially for the wall thinning at the extrados. This paper analyses the wall thickness distribution in an integrated tube bending and spinning process, investigating various levels of the complexity to reveal the possibility of the proposed combined process. The coupling of bending and spinning and influence on the wall thickness distribution are investigated.

A finite element model was established based on the ABAQUS software and test data. Mechanical performance of the tube was tested under uniaxial tension. The values of wall thickness distribution were taken at bending angles of 15° to 90° for both stainless steel and steel alloys. The study also took into account the factor of friction between the inner and outer clamps, which varied from 0.1-0.5. The location where the neutral axis shifted was measured using the percentage change in wall thickness, both in maximum and minimum percent values were calculated using the following equation [16]:

$$\%\,\textbf{Wall Thickness Distribution} = \frac{t_{new} - t_o}{t_o} \times 100 \quad (5)$$

Where t_{new} represents the new thickness of the tube, and t_o is the original thickness. Consequently, the percentage change in wall thickness is negative at the outer arc and positive at the inner arc.

The results in Table 4 show that the maximum wall thickness values in stainless steel alloys fluctuate slightly as the coefficient of friction increases. At a 90° bending angle, the maximum thickness ranges from 13.331% at a friction coefficient of 0.1 to 13.493% at a coefficient of 0.5. This indicates that friction between the clamps does not significantly impact the maximum wall thickness in stainless steel alloys. However, the minimum wall thickness values display a more consistent decrease as the bending angle increases. At the 90° angle, the minimum thickness ranges from -14.376% at a 0.1 coefficient of friction to -15.0768% at a 0.5 coefficient. These changes are compounded by the increase in temperature due to friction, which can soften the material, leading to slightly greater thinning in areas subjected to higher heat.

While the maximum thickness remains relatively stable, the degree of wall thinning at the outer arc of the tube becomes more pronounced as friction increases. The variations in maximum and minimum wall thicknesses suggest that higher friction coefficients may not dramatically affect the extremes in wall thickness for stainless steel alloys. However, at higher friction coefficients, along

with the associated temperature rise, may slightly increase material deformation, especially at larger bending angles.

Table 4. Extremes of wall thickness distribution in stainless steel alloys at different bending angles and friction values between inner and outer clamps.

Bending Angle (º)			15º	30º	45º	60º	75º	90º
Coefficient of Friction Between Clamps	0.1	Max	8.238	11.7215	15.055	15.4055	15.3645	13.331
		Min	-6.3685	-11.8015	-13.1815	-13.218	-13.56	-14.376
	0.2	Max	7.957	11.6955	12.464	12.494	14.481	7.651
		Min	-5.989	-9.842	-12.599	-12.6235	-14.1875	-6.277
	0.3	Max	7.651	11.5045	12.4185	13.5235	13.948	13.8935
		Min	-6.277	-12.049	-12.6415	-13.7705	-14.676	-14.7685
	0.4	Max	8.3225	10.9595	12.546	13.314	13.7385	13.635
		Min	-6.3685	-12.905	-12.6215	-13.692	-14.7075	-15.2545
	0.5	Max	8.4055	11.138	12.413	13.08	11.993	13.493
		Min	-6.3845	-12.604	-12.6545	-13.7985	-15.0755	-15.0768

In contrast, Table 5 presents the wall thickness distribution in steel alloys under similar conditions. Unlike stainless steel, steel alloys exhibit more significant variations in maximum wall thickness with changes in the coefficient of friction. At a 90° bending angle, the maximum thickness decreases from 17.164% at a friction coefficient of 0.1 to 16.8755% at a coefficient of 0.5, indicating a slight reduction in thickness as friction increases. The friction between the clamps, combined with the heat generated, has a more substantial impact on the structural integrity of steel alloys, leading to greater variations in wall thickness. The heat effect is particularly important here, as steel alloys are more sensitive to temperature changes, which may accelerate softening and deformation.

Likewise, in steel alloys, the minimum wall thickness values decrease with the bending angle, but this decrease is more pronounced when compared with the stainless steel. This minimum thickness is reduced from -19.9088% (CF = 0.1) to -20.039% (CF = 0.5) under the 90° bending angle. This increased thinning of the wall makes the effect of friction higher in steel alloys, particularly at higher bending angles. The results indicate that the formability of steel Alloys are more sensitive to the coefficient of friction than stainless steel. The decrease is more significant at higher bending angles, suggesting that regulating the friction is more important for keeping wall continuity of steel alloys.

Table 5. Bounds of the wall thickness distribution in steel alloys under various bending angles and friction conditions between inner and outer clamps.

Bending Angle (º)			15º	30º	45º	60º	75º	90º
Coefficient of Friction Between	0.1	Max.	9.725	12.915	9.291	15.1065	16.7705	17.164
		Min.	-10.5455	-20.95	-25.156	-23.011	-19.9085	-19.9088
	0.2	Max.	3.143	3.14	15.193	17.3345	18.0635	19.278
		Min.	-4.5075	-4.5075	-23.5835	-20.054	-18.0645	-19.318

	0.3	Max.	0.0595	5.1955	7.278	14.6185	14.6212	16.9655
		Min.	-1.3715	-18.711	-23.1835	-22.975	-22.978	-19.999
	0.4	Max.	0.5875	1.4775	8.393	13.148	16.1805	16.692
		Min.	-3.671	-9.3345	-25.001	-24.5755	-19.083	-19.7005
	0.5	Max.	0.4015	0.128	0.074	8.719	16.1555	16.8755
		Min.	-2.8205	-4.236	-11.9565	-25.371	-19.399	-20.039

Both the stainless steel and steel alloy change in wall thickness, but the steel alloy has a greater change in wall thickness for varying coefficients of friction. The maximum wall thickness that can be achieved with the stainless steel is approximately consistent for various coefficients of friction, but that is not the case for the steel alloys, demonstrating a larger sensitivity to friction. Moreover, the minimum wall thickness of the steel alloys decreases more significantly with increasing bending angles than stainless steel, so steel alloys may be more vulnerable to the wall thinning phenomenon during the bending operation. These results emphasize the need to control more accurately the frictional conditions in the case of working on steel alloys to have the bent tube having the expected dimensions, contrary to the stainless steel alloys which were less sensitive to the change in the friction compared to steel alloys.

Generally, the comparison between both tables indicates how material choice and process tuning affect the tube bending. Stainless steel grades are more resistant than those in the mild range; however, they may undergo about the same deflection in ratio to the wall thickness. In comparison to TRC, steel base alloys are more susceptible to friction and wall thinning; therefore more attention should be given to the control of the frictional variables and parameters to guarantee the quality and integrity of the final product.

Mechanical Characteristics of materials greatly affect the translocation of the neutral axis, the change in thickness distribution, and strain distribution during bending. A sophisticated geometric model was proposed to enable a precise characterization of these effects and concentrated in particular on neutral axis displacement and the concomitant wall-thickness distribution in the tube [32]. The longitudinal strain causing these changes can be divided into two aspects: tensile strain, which dominated in the middle of the tube, and bending strain, which was the main part on the top and bottom of the tube.

At first, the position of the neutral axis is in the geometrical center of the tube and from this point to the center of the forming die is the bending radius (Rb). There is also offset in the position of the tube neutral axis as bending unfolds (05) which creates new post-shift bending radius. The position of a point on a tube relative to the center line, with being a displacement, is obtained in dependence of the angle with reference to the neutral surface; see.

The measurement of neutral axis shifting and wall thickness distribution was obtained through a time-dependent simulation of the model. The simulation was conducted over 157 seconds, during which the tube was progressively bent to a maximum angle of 90 degrees. Any occurrence of ovalization or structural failure of the tube during this bending process was classified as a process failure. The results of the simulation provide a detailed analysis of the neutral axis shifting and wall thickness distribution at various bending angles, ranging from 15° to 90°, for both stainless steel and steel alloys. The simulations were conducted under varying coefficients of friction between the inner and outer clamps, with values ranging from 0.1 to 0.5. Figure 4 presented in this study, generated using the ABAQUS software, illustrate the outcomes of these simulations. As friction increases, the neutral axis shift becomes more pronounced. The heat generated due to

increased friction also plays a role in this shift. At higher temperatures, the material yield strength can decrease, making it more susceptible to deformation.

In Figure 4 (a), corresponding to a friction coefficient of 0.1, both stainless steel and steel exhibit an increase in neutral axis shifting with rising bending angles. At this low friction level, the shift in the neutral axis is relatively modest. The mechanical properties of stainless steel enable a more controlled and uniform shift compared to the steel alloy. This predictability can be attributed to the inherent strength and ductility of stainless steel, which allow it to maintain structural integrity even under bending forces. The minimal friction results in smoother bending, which limits the extent of the neutral axis displacement. However, the extent of the shift is more pronounced in steel alloys compared to stainless steel. This suggests that, at a lower friction coefficient, steel alloys are more sensitive to bending, resulting in a greater shift of the neutral axis towards the inner arc of the tube.

As the friction coefficient increases to 0.2, Figure 4 (b), the neutral axis shifting becomes more pronounced. The friction coefficient influences the bending dynamics by introducing additional resistance against the material deformation. This resistance causes more significant shifts in the neutral axis for both materials. The distribution of wall thickness starts to exhibit variations, and the material differences become increasingly significant. Stainless steel continues to demonstrate a more predictable shift in the neutral axis, while the steel alloy begins to display greater variability , indicating that as friction increases, the sensitivity of steel alloys to bending intensifies.

When friction coefficient rises to 0.3, shift of the neutral axis is more obvious, which means the bending process becomes more complex and more difficult to control, Figure 4 (c). The increased friction increases deformation resistance and hence an even greater movement toward the inner tube arc. Whereas such a shift is seen in both materials, the stainless steel shows better control of this than the steel alloy. The behavior discrepancy between materials in this friction conditiongrowth is the increase in the differences in behavior between the two materials, which the steel alloy is much more influenced by the bending action. Moreover, this level of friction would cause non uniform wall thickness distribution and greater possibility of failure, especially for the steel alloys. This shows how material choice and the control of friction are key for bending.

From Figure 4(d), it is evident that the neutral axis shifts further for stainless steels and steel alloys at a friction coefficient of 0.4. The higher friction adds another level of complexity to the bending of the fibre, causing the neutral axis to move further towards the inner arc. With such high friction conditions, maintaining structural integrity is difficult and both materials show signs of possible ovalisation and uneven wall thickness distribution. Though stainless steel in general has a higher performance than the steel alloy, it starts to fail to control the shift at this high friction level. This indicates that the bending process tends to be more vulnerable to the structural trouble as the friction increases, highlighting the importance of adequate friction control to alleviate the risk.

The highest-neutral-axis shift also is maximum at the highest friction coefficient, 0.5 (Fig. 4(e)). The high friction and heat generates the more difficulty to sustain its constriction integrity. Significant changes and the resulting, emergence of process failure is observed for both stainless steal and steel alloys. The distribution of the wall thickness is extremely non-uniform, and ovalization tendencies are much aggravated and the like. Although stainless steel still provides a better axial shift control performance compared to the steel alloy, it has already started to become unstable in this high level of friction.

In all cases stainless steel presents a more restrained and predictable shift of the neutral axis in comparison to steel alloys, especially in the lower ones (0.1 and 0.2). Both magnetic softness and

hardeness have very large movements as friction grows up, in particular they show the greatest movements at the largest coefficient of 0.5. The results suggest that higher friction further aggravates these shifts, exhibiting more gradual transitions with lower friction, while more pronounced structural hurdles (e.g., ovalization) are recognized at greater levels, primarily in the case of the steel alloys. Although the trend for the stainless steel is more influenced by the neutral axis shift, both materials are greatly influenced by the rising level of friction. These results highlight the importance of accurate friction control in order to minimize structural failures and achieve bending tune-ability.

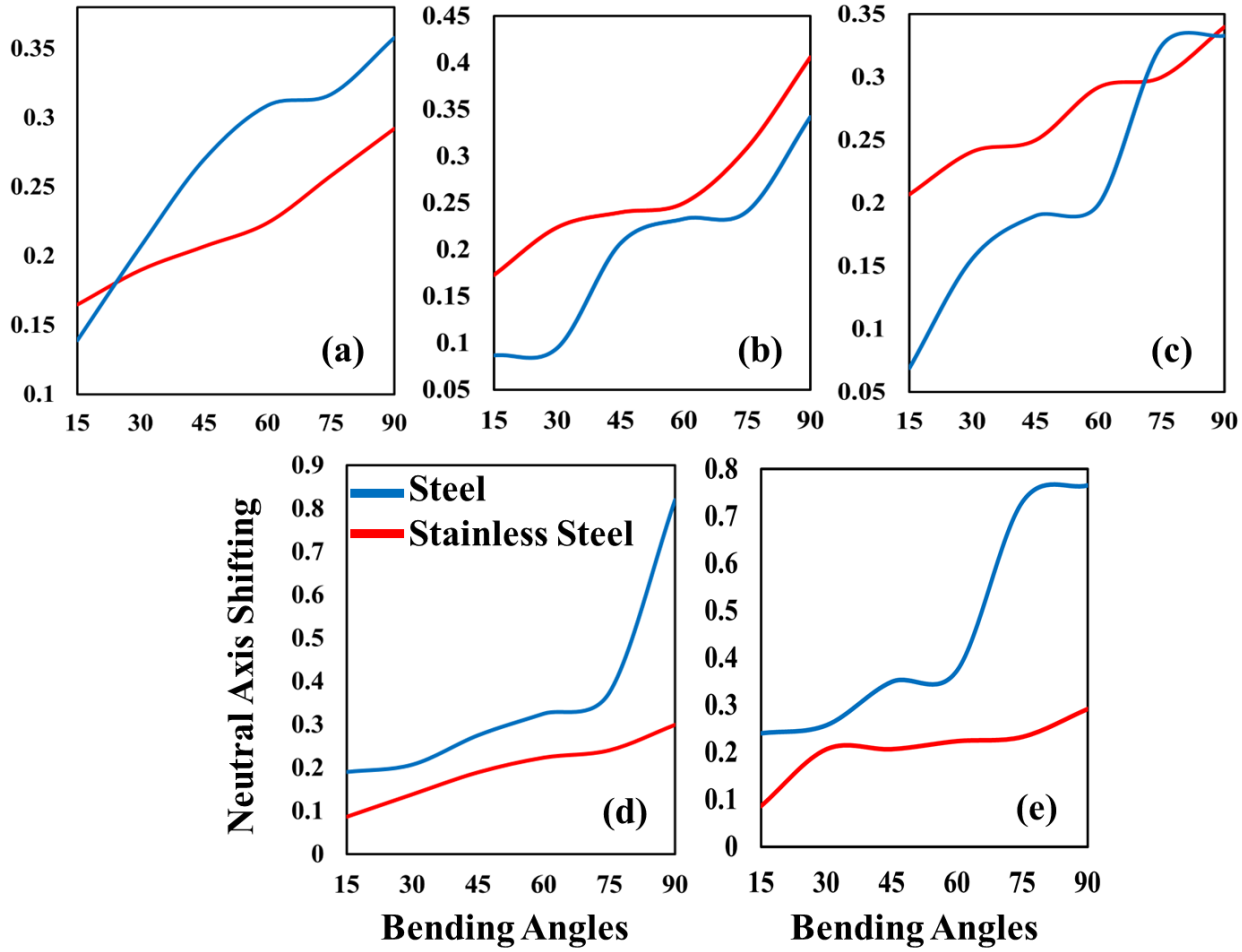

Figure 4. Shift in neutral axis at different bending angles for clamping dies made of both stainless steel alloy and alloy steel for different values of friction: (a) 0.1, (b) 0.2, (c) 0.3, (d) 0.4, and (e) 0.5.

Conclusions

This paper offers useful information for the influence of different friction conditions ranging from 0.1 to 0.5 on the tube bending, specifically, involving the neutral axis shifting and the wall thickness distribution in tube bending from 15° to 90°. Based on ABAQUS simulations, the study reveals the different tendencies of the SS and steel alloys. Stainless steel demonstrates relatively stable performance, with maximum wall thickness values changing slightly from 13.331% to 13.493% as friction increases, while steel alloys show greater sensitivity, with maximum thickness decreasing from 17.164% to 16.8755%. Additionally, neutral axis shifting in steel alloys increases more significantly with friction, from 0.13 mm at 0.1 friction and 15° bending to 0.8 at 0.5 friction and 90° bending, indicating a greater susceptibility to deformation. The findings emphasize the importance of optimizing friction parameters, particularly for steel alloys, to minimize structural failures and ensure the quality of bent tubes in industrial applications. These

results offer valuable guidance for improving the efficiency and precision of metal forming processes.

Funding

This research received no specific grant from any funding agency in the public, commercial, or not-for-profit sectors.

Conflict of Interest

"The authors indicate that they have no financial conflicts of interest or personal connections that might have inappropriately influenced (biased) their work in this study".

Ethical Approval

Since this was a laboratory study and no humans/animals or clinical trials are involved the section is not applicable.

Data Availability

The experimental findings and research data produced in this study are available from the corresponding author upon request in accordance with the formal request system.

Contributions

- Hassan Raheem Hassan: Conceptualization, Methodology, Software, Formal Analysis, Writing – Original Draft.
- Muhannad Altimemy: Validation, Investigation, Data Curation, Visualization.
- Mustafa Jabbar Hayawi: Resources, Writing – Review & Editing, Supervision.

Acknowledgments

The authors acknowledge the College of Engineering, Al-Shatrah University, Thi-Qar, Iraq, for providing computational resources and technical support.

Disclosure

This manuscript is original, has not been published elsewhere, and is not under consideration by another journal.

References

1. J. Li, C.Y. Zhou, P. Cui, X.H. He, Plastic limit loads for pipe bends under combined bending and torsion moment, Int. J. Mech. Sci. 92 (2015) 133–145. doi: 10.1016/j.ijmecsci.2014.12.011.
2. Y. Hea, L. Heng, Z. Zhiyong, Z. Mei, L. Jing, L. Guangjun, Advances and trends on tube bending forming technologies, Chinese J. Aeronaut. 25 (2012) 1–12. doi:10.1016/S1000-9361(11)60356-7.
3. L. Heng, Y. He, Z. Mei, S. Zhichao, G. Ruijie, Role of mandrel in NC precision bending process of thin-walled tube, Int. J. Mach. Tools Manuf. 47 (2007) 1164-I 175. doi:doi: 10.1016/j.ijrnachtools.2006.09.001.
4. Daxin E, Y. Liu, Springback and time-dependent springback of 1Cr18Ni9Ti stainless steel tubes under bending, Mater. Des. 31 (2010) 1256–1261. doi:10.1016/j.matdes.2009.09.026.
5. Z.Q. Jiang, H. Yang, M. Zhan, X.D. Xu, G.J. Li, Coupling effects of material properties and the bending angle on the springback angle of a titanium alloy tube during numerically controlled bending, Mater. Des. 31 (2010) 2001–2010. doi:10.1016/j.matdes.2009.10.029.

6. G.Y. Zhao, Y.L. Liu, C.S. Dong, H. Yang, X.G. Fan, Analysis of wrinkling limit of rotary-draw bending process for thin-walled rectangular tube, J. Mater. Process. Technol. 210 (2010) 1224–1231. doi:10.1016/j.jmatprotec.2010.03.009.
7. J.E. Miller, S. Kyriakides, E. Corona, On bend-stretch forming of aluminum extruded tubes - II: analysis, Int. J. Mech. Sci. 43 (2001) 1283–1317. doi:10.1016/S0020-7403(00)00039-4.
8. S. Kyriakides, E. Corona, J.E. Miller, Effect of yield surface evolution on bending induced cross sectional deformation of thin-walled sections, Int. J. Plast. 20 (2004) 607–618. doi:10.1016/S0749-6419(03)00075-5.
9. J. Wang, R. Agarwal, Tube bending under axial force and internal pressure, J. Manuf. Sci. Eng. 128 (2006) 598–605. doi:10.1115/1.2112987.
10. N.C. Tang, Plastic-deformation analysis in tube bending, Int. J. Press. Vessel. Pip. 77 (2000) 751–759. doi:10.1016/S0308-0161(00)00061-2.
11. C.K. Oh, Y.J. Kim, C.Y. Park, Effects of local wall thinning on net-section limit loads for pipes under combined pressure and bending, Nucl. Eng. Des. 239 (2009) 261–273. doi:10.1016/j.nucengdes.2008.10.019.
12. H. Lee, C.J.V. Tyne, D. Field, Finite element bending analysis of oval tubes using rotary draw bender for hydroforming applications, J. Mater. Process. Technol. 168 (2005) 327–335. doi:10.1016/j.jmatprotec.2004.11.019.
13. L. Heng, Y. He, A study on multi-defect constrained bendability of thin-walled tube NC bending under different clearance, Chinese J. Aeronaut. 24 (2011) I 02-112.
14. H. Li, H. Yang, M. Zhan, R.J. Gu, Forming characteristics of thin-walled tube bending process with small bending radius, Trans. Nonferrous Met. Soc. China (English Ed. 16 (2006) s613–s623. doi:10.1016/S1003-6326(06)60266-5.
15. S. Kajikawa, G. Wang, T. Kuboki, Prevention of defects by optimizing mandrel position and shape in rotary draw bending of copper tube with thin wall, Procedia Manuf. 15 (2018) 828–835.
16. B. Engel, H.R. Hassan, Investigation of neutral axis shifting in rotary draw bending processes for tubes, Steel Res. Int. 85 (2014) 1209–1214. doi:10.1002/srin.201300333.
17. E. Daxin, Y. Liu, H. Feng, Deformation analysis for the rotary draw bending process of circular tubes: stress distribution and wall thinning, Steel Res. Int. 81 (2010) 1084–1088. doi:10.1002/srin.201000109.
18. H. Li, H. Yang, J. Yan, M. Zhan, Numerical study on deformation behaviors of thin-walled tube NC bending with large diameter and small bending radius, Comput. Mater. Sci. 45 (2009) 921–934. doi:doi: 10.1016/j.commatsci.2008.12.018.
19. D. Maier, S. Stebner, A. Ismail, M. Dölz, B. Lohmann, S. Münstermann, W. Volk, The influence of freeform bending process parameters on residual stresses for steel tubes, Adv. Ind. Manuf. Eng. 2 (2021). doi:10.1016/j.aime.2021.100047.
20. E. Simonetto, A. Ghiotti, S. Bruschi, Dynamic detection of tubes wrinkling in three roll push bending, Procedia Eng. 207 (2017) 2316–2321. doi:10.1016/j.proeng.2017.10.1001.
21. J. Chen, E. Daxin, J. Zhang, Effects of process parameters on wrinkling of thin-walled circular tube under rotary draw bending, Int. J. Adv. Manuf. Technol. 68 (2013) 1505–1516. doi:10.1007/s00170-013-4938-5.

22. H. Li, H. Yang, M. Zhan, R.J. Gu, The interactive effects of wrinkling and other defects in thin-walled tube NC bending process, J. Mater. Process. Technol. 187–188 (2007) 502–507. doi:doi:10.1016/j.jmatprotec.2006.11.100.

23. Breaking through the bending limit of al-alloy tubes by cryogenic effect controlled mechanical properties and friction behaviours, Int. J. Mach. Tools Manuf. 195 (2024). doi:doi.org/10.1016/j.ijmachtools.2023.104111.

24. C. Cheng, G. Wei, H. Zhang, Z. Ma, J. Tao, C. Liu, X. Guo, Theoretical analysis, finite element modeling and experimental investigation of the impact of friction between tube and bending die on the formability of the tube during the free-bending process, CIRP J. Manuf. Sci. Technol. 44 (2023) 104–115. doi:doi.org/10.1016/j.cirpj.2023.05.003.

25. J. Wu, Z. Zhang, Q. Shang, F. Li, Y. Wang, Y. Hui, H. Fan, A method for investigating the springback behavior of 3D tubes, Int. J. Mech. Sci. 131–132 (2017) 191–204. doi:dx.doi.org/10.1 0l 6/j.ijmecsci.2017 .06.047.

26. Z.K. Zhang, J.J. Wu, R.C. Guo, M.Z. Wang, F.F. Li, S.C. Guo, Y. Wang, W.P. Liu, A semi-analytical method for the springback prediction of thick-walled 3D tubes, Mater. Des. 99 (2016) 57–67. doi:dx.doi.org/10.1016/j.matdes.2016.03.026.

27. E. Daxin, M. Chen, Numerical solution of thin-walled tube bending springback with exponential hardening law, Steel Res. Int. 81 (2010) 286–291. doi:10.1002/srin.200900122.

28. H. Li, H. Yang, F.F. Song, M. Zhan, G.J. Li, Springback characterization and behaviors of high-strength Ti-3Al-2.5V tube in cold rotary draw bending, J. Mater. Process. Technol. 212 (2012) 1973–1987. doi:dx.doi.org/10.1016/j.jmatprotec.2012.04.022.

29. S.A. Tronvoll, J. Ma, T. Welo, Deformation behavior in tube bending: a comparative study of compression bending and rotary draw bending, Int. J. Adv. Manuf. Technol. 124 (2023) 801–816. doi:10.1007/s00170-022-10433-7.

30. B. Engel, H. Hassan, The influence of material properties on rotary draw bending processes, (2014) 8–12.

31. H. Yang, R.J. Gu, M. Zhan, H. Li, Effect of frictions on cross section quality of thin-walled tube NC bending, Trans. Nonferrous Met. Soc. China (English Ed. 16 (2006) 878–886. doi:10.1016/S1003-6326(06)60344-0.

32. B. Engel, H. Hassan, Advanced model for calculation of the neutral axis shifting and the wall thickness distribution in rotary draw bending processes, Int. J. Mater. Metall. Eng. 9 (2015) 239–243.

33. Altimemy, M., Ibrhim, A.K., Hassan, H.R., Hayawi, M.J., Computational Study of Pump Turbine Performance Operating at Off-Design Condition-Part I: Vortex Rope Dynamic Effects, CFD LettersThis link is disabled., 2025, 17(3), pp. 148–166

34. Cao, F., Al-Bahrani, M., Smait, D.A., ... Nasajpour-Esfahani, N., Hekmatifar, M., Effective parameters on the combustion performance of coated aluminum hydride nanoparticles: A molecular dynamics study, Materials Today CommunicationsThis link is disabled., 2023, 36, 106586

35. Hasan, H., Egab, K., Hassan, H., Thermal and hydraulic characteristics study of different dimpled micro-channel heat sinks, AIP Conference ProceedingsThis link is disabled., 2021, 2404, 080009

36. Egab, K., Oudah, S.K., Nassar, A.A., Hassan, H.R., Bhuiyan, Y., Investigation of temperature effect on cracked pressurized pipes, ASME International Mechanical Engineering Congress and Exposition, Proceedings (IMECE), 2018, 4A-2018